Supporting Information For

Flexible Nano-Cloth-like Ag cluster@rGO with Ultrahigh SERS Sensitivity for Capture-Optimization-Detection due to Effective Molecule-Substrate Interaction

Yanying Cui,[a] Linan Xu,[b] Haitao Li,[c] Xuan Wang,[a] Fuwei Sun,[d] Huan Wang,[c] Xinguang Guo,[e] Zhang Yihe,[a] Hongbo Gao,*[e] Qi An*[a]*

[a]*State Key Laboratory of Geological Processes & Mineral Resources, National Laboratory of Mineral Materials, School of Materials Science and Technology, China University of Geosciences (Beijing), Beijing 100083, China.*

[b]*College of Materials Engineering, North China Institute of Aerospace Engineering, Langfang 065000, China.*

[c]*School of Chemistry and Chemical Engineering, Yangzhou University, Yangzhou, 225002, PR China.*

[d]*Chemistry department, Tsinghua University, 100084, P. R. China.*

[e]*China National Institute of Food and Fermentation Industries Co, Ltd, Beijing 100015, China.*

*Corresponding authors: htli@yzu.edu.cn (Haitao Li); 15011559852@139.com (Hongbo Gao); an@cugb.edu.cn (Qi An)

Section S1.

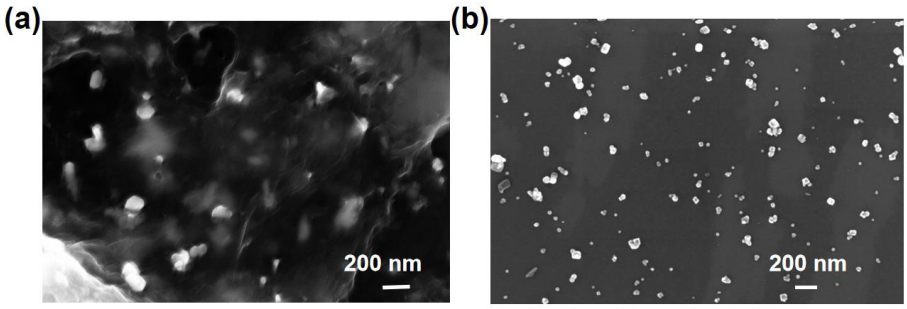

Figure S1. Exploring the morphology of composite materials under different conditions. SEM images of **(a)** GO reacts with $AgNO_3$. **(b)** PEI reacts with $AgNO_3$.

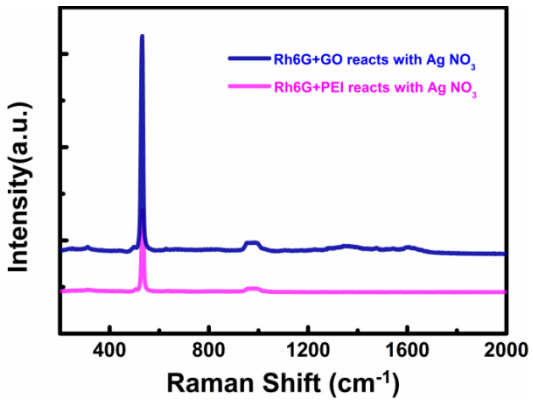

Figure S2. SERS detection performance in only PEI and GO react with $AgNO_3$.

Section S2.

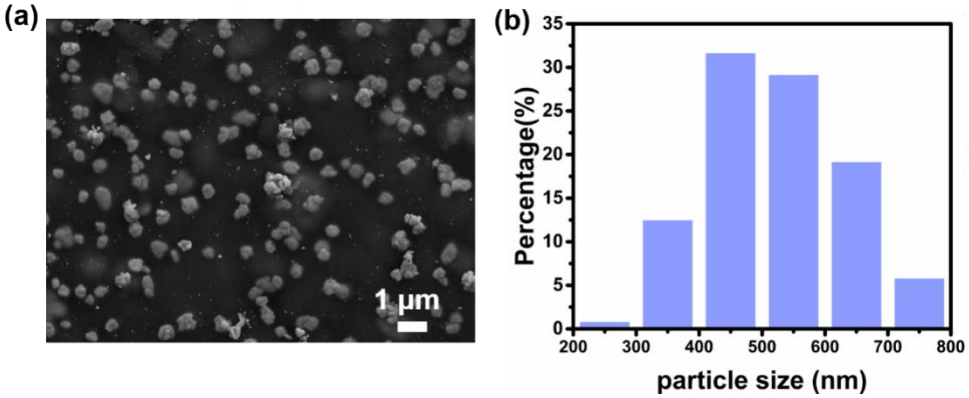

Figure S3. **(a)** SEM image of Ag cluster@rGO, and **(b)** the related size distributions on the Ag clusters loading on rGO-PEI.

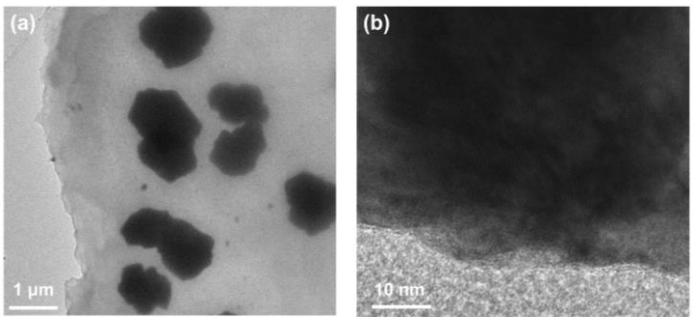

Figure S4. **(a)** TEM image of Ag cluster@rGO, **(b)** the corresponding magnified image.

Flower-like Ag clusters possess typical sharp edges and narrow gaps between each other, which are favorable for achieving superior "hot spot", leading to the enhancement of Raman signals on analytes, as presented in **Figure S4.**

Section S3. Analysis of the formation of Ag cluster structure.

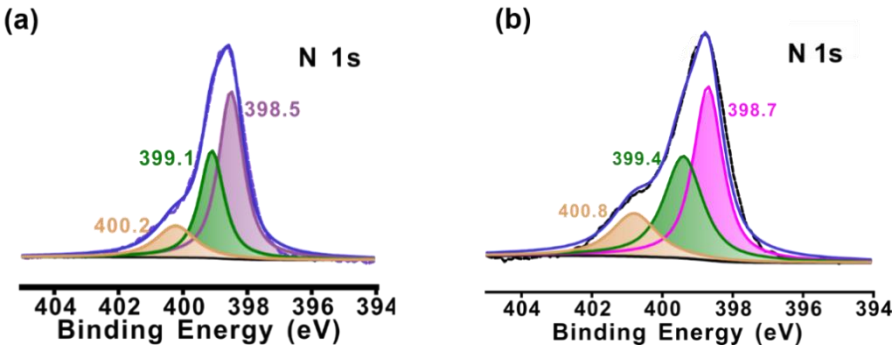

Figure S5 (a-b) High-resolution XPS spectrum of N1s in rGO-PEI and Ag cluster@rGO-PEI.

The selected PEI modified on graphene, with numerous amine groups, allows effectively adsorbing Ag^+ ion from solution and subsequently provides the reducing power for the generation of Ag clusters (*Nano Energy,* 2022, **92**, 106737). Moreover, to study the change of PEI layer after Ag nanoparticle formation, high-resolution XPS spectrum of N1s in rGO-PEI and Ag cluster@rGO have been deeply analyzed in Figure **Figure S5. Figure S5 (a)** indicates that there are observed three peaks at 398.5, 399.1 and 400.2 eV, which belong to C-N=C, -NH_2 and C-NH respectively (*Adv. Funct. Mater.* 2018, **28**, 1800668-1800677). While after the Ag nanoparticle formation, the related peak at 398.5 eV shifts to 398.7 eV, 399.1 eV slightly shifts to 399.4 eV and 400.2 eV shifts to 400.8 eV, respectively, in following **Figure S5 (b)**, suggesting the existence of the binding ability between Ag and N.

Section S4.

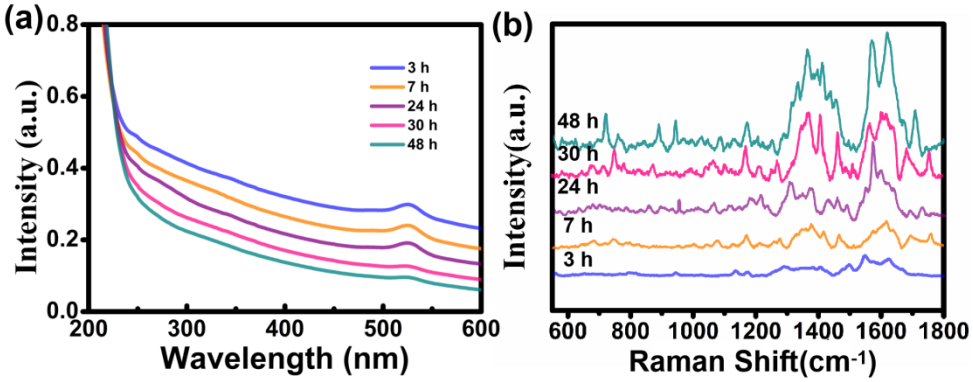

Figure S6 (a) UV-vis spectra of the supernatant of Ag cluster@rGO (1 mg/mL) mixed with Rh6G (10^{-6} M) solution for 3 h, 7h, 24h, 30h and 48h, respectively. (b) SERS intensity of Rh6G changed with time (3 h, 7 h, 24 h, 30 h, and 48 h, respectively)

Section S5.

To demonstrate the importance of Ag cluster@rGO for enhanced charge transfer, three control experiments, using Ag nanoparticles only, rGO-PEI only, and physical mixing of Ag and rGO as SERS substrate to detect Rh6G (10^{-6} M), respectively, have been conducted.

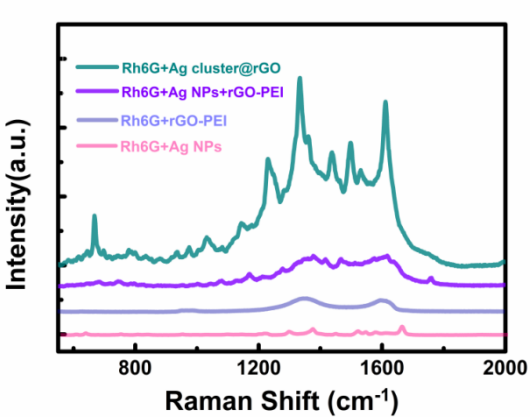

Figure S7. The SERS spectra of Rh6G in different substrates (Ag NPs, rGO-PEI, Ag+rGO-PEI and Ag cluster@rGO, respectively).

The Raman signals for Rh6G detected from Ag nanoparticles only and physical mixing of Ag and rGO show almost the same spectral intensity, indicating that they have similar SERS enhancement effect. And the Rh6G Raman signal can be hardly detected from rGO-PEI based substrate. Compared to other design, obviously our reported Ag cluster@rGO, where chemically tethering Ag onto rGO, display a highest SERS signal. Therefore, abovementioned results suggest that such typical Ag cluster@rGO possess superior SERS performance, owing to the synergistic effect of Ag and rGO-PEI via their typical chemical bonding, which beneficial to enhanced charge transfer.

Section S6. Charge distribution of BPA.

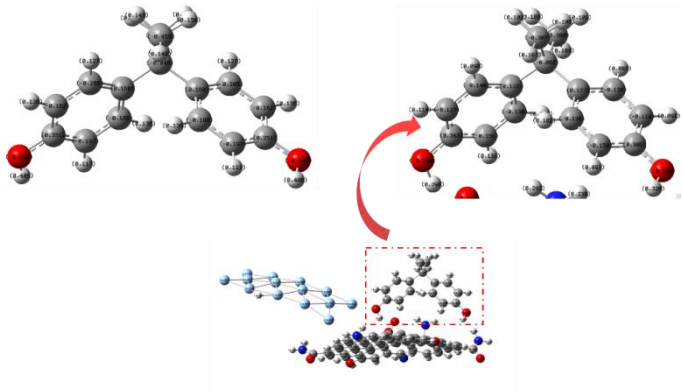

Figure S8 The number of charges on each atom of pure BPA and the BPA of Ag cluster@rGO@BPA composite system

Table S1. Charge distribution

Atomic number	BPA	BPA (Ag cluster @rGO@BPA)
1	-0.646	-0.598
2	-0.646	-0.556
3	-0.048	-0.065
4	0.160	0.132
5	0.160	0.127
6	-0.455	0.308
7	-0.455	-0.307
8	-0.185	-0.130
9	-0.185	-0.130
10	-0.205	-0.140
11	-0.205	-0.138
12	-0.197	-0.156
13	-0.197	-0.150
14	-0.162	-0.127
15	-0.162	-0.114
16	0.351	0.343
17	0.351	0.306
18	0.143	-0.308
19	0.149	0.101
20	0.150	0.106
21	0.150	0.105
22	0.143	0.101
23	0.149	0.107
24	0.136	0.102
25	0.136	0.102
26	0.127	0.090
27	0.127	0.083
28	0.117	0.131
29	0.117	0.097
30	0.136	0.119
31	0.136	0.091
32	0.406	0.390
33	0.406	0.320

After the formation of Ag cluster@rGO@BPA composite system, the number of charges around each atom of BPA have changed greatly, caused by the charge transfer between the BPA molecule and the Ag cluster@rGO substrate.

Section S7. Optimized molecular structures and characteristic SERS bands of BPA derivatives and assignments.

Calculation of the molecular theoretical Raman spactras were carried out using the unrestricted B3LYP exchange-correlation functional, as implemented in the Gaussian 09 computational chemistry package. The 6-31G (d, p) basis set was used for all atoms.

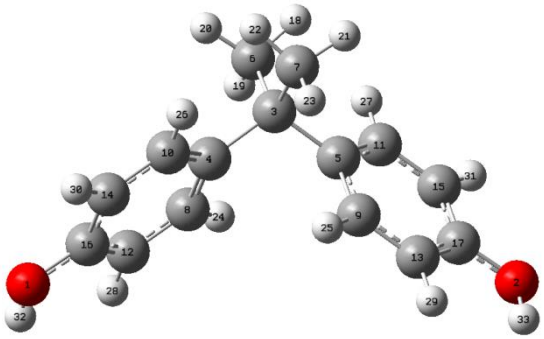

Figure S9. Optimized molecular structure and numbers of individual atoms of BADGE.

Table S2. Experimental SERS Characteristic and calculated of BADGE and assignments.

Calculated/cm^{-1}	SERS/cm^{-1}	Assignments
370		γ-CH_3
531	528	γ-CH_3、γ $O_2C_6C_{10}$、γ-benzene ring
736	734	γ-benzene ring
840		γ-benzene ring、γ-$H_{41\text{-}48}$/$H_{27\text{-}30}$
859	866	ν-benzene ring、ν-$O_{3\text{-}4}$、γ -CH_3
973	963	ν-CH_3、γ-H_{42}/H_{46}
1030	1037	γ-CH_3
1160	1175	γ-H_{25}/H_{27}/H_{28}
1230	1220	δ-$H_{41\text{-}48}$
1291	1294	ν-benzene ring、ν-$C_5C_9C_{13}$
1350	1336	ν-$C_8C_{16}C_{18}C_{22}C_{28}$
1384	1391	ν-$C_5C_9O_1$、δ-$H_{25/27/28/37/38}$
1462	1471	ν-benzene ring、δ-$H_{18\text{-}33}$
1520	1536	ν-CH_3
1630		ν-benzene ring
1670		ν-benzene ring、γ-$H_{37\text{-}40}$

ν(stretching vibration), γ(wagging vibration), δ(in plane wagging vibration),C_x(Number of carbon atom in the molecule),H_x(Number of hydrogen atom in the molecule),O_x(Nnumber of the oxygen atom in the molecule).

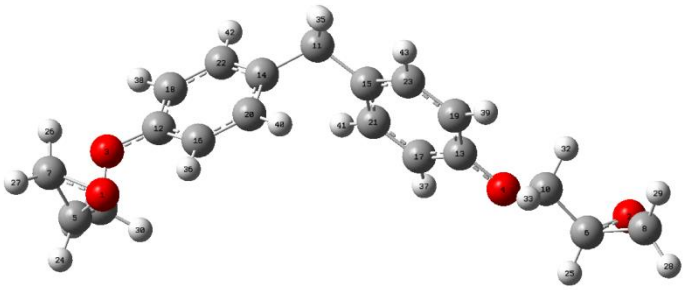

Figure S10. Optimized molecular structure and numbers of individual atoms of BFDGE.

Table S3. Experimental SERS Characteristic and calculated of BFDGE and assignments.

Calculated/cm^{-1}	SERS/cm^{-1}	Assignments
360		$\gamma O_2C_6C_8/O_1C_5C_7$、$\gamma$-$CH_3$、$\gamma$-benzene ring
656	712	ν-benzene ring、γ-$C_5/C_7/C_9$
784	802	γ-benzene ring、 δ-H_{36-43}
840		ring breathing、γ-H_{36-43}
672		γ-benzene ring
960	979	γ-H_{36-43}、γ-$H_{34/35}$
1176	1163	γ-H_{24-33}、γ-$O_2C_6C_8/O_1C_5C_7$
1208		δ-H_{36-43}
1296		γ-H_{24-29}
1320	1346	ν-benzene ring、γ-$H_{31/38}$、δ-$H_{36/38/40/42}$
1368	1420	ν-benzene ring、γ-$H_{34/35}$
1496		γ-$H_{30/31/34/35}$
1560	1510	ν-benzene ring、γ-H_{24-35}、δ-H_{36-43}
1632	1571	ν-benzene ring、γ-$H_{34/35}$
1672	1626	ν-benzene ring

ν(stretching vibration), γ(wagging vibration), δ(in plane wagging vibration),C_x(Number of carbon atom in the molecule),H_x(Number of hydrogen atom in the molecule),O_x(Nnumber of the oxygen atom in the molecule).

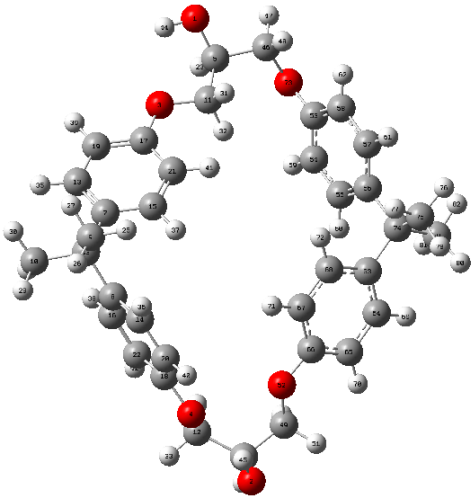

Figure S11. Optimized molecular structure and numbers of individual atoms of Cdb.

Table S4. Experimental SERS Characteristic and calculated of Cdb and assignments.

Calculated/cm^{-1}	SERS/cm^{-1}	Assignments
569	570	γ-ringC_{53}、 ringC_{63}
655	655	δ-ringC_7/ringC_8/ringC_{53}/ ringC_{63}
785	782	δ-ringC_7/ringC_8/ringC_{53}/ ringC_{63} γ-$H_{25\text{-}30}$/$H_{25\text{-}30/76\text{-}78/80\text{-}82}$
855	854	γ-ringC_{53}、 γ-$H_{59/60/71/72}$
973	981	γ-$H_{59/60}$
1012	1005	γ-$C_{12\text{-}6\text{-}49}$、γ-$H_{24/33/34}$
1066	1066	ν-ringC_7/ringC_{53}、 ν-C_{46}-O_{73}
1146	1145	δ-$H_{59\text{-}62/69\text{-}72}$
1208	1203	δ-$H_{59\text{-}62/69\text{-}72/35/37/39/41}$
1215	1223	δ-$H_{35\text{-}42}$
1253	1247	δ-$H_{74/75/79}$、δ-ringC_{53}/ringC_{63}、δ-$H7_{6\text{-}78/80\text{-}82}$
1306	1312	ν-ringC_{53}、γ-$H_{31/3223/44/47/48}$
1347	1346	δ-ringC_8
1377	1377	ν-$C_{11\text{-}5\text{-}46}$、γ-$H_{23/32/47/48}$
1514	1514	ν-benzene ring、δ-$H_{24\text{-}31}$
1559	1562	δ-ringC_8、δ-$H_{35\text{-}42}$
1624	1617	δ-ringC_{53}

ν(stretching vibration), γ(wagging vibration), δ(in plane wagging vibration), C_x (Number of carbon atom in the molecule), H_x(Number of hydrogen atom in the molecule), O_x(Nnumber of the oxygen atom in the molecule).

Section S8.

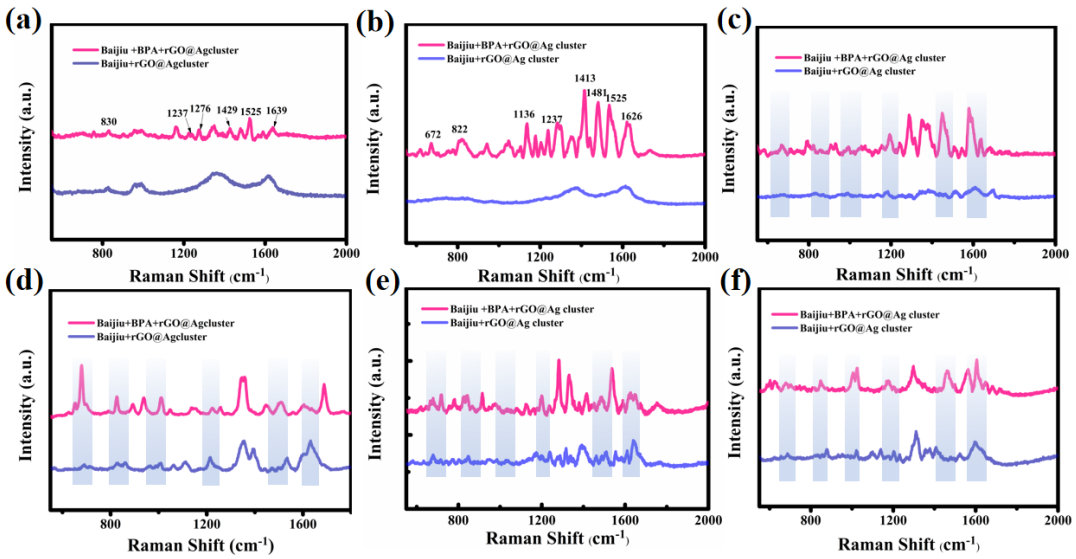

Figure S12. SERS spectrum of six types of Baijiu. (a-b) Negative samples (Baijiu with no detectable contaminants). (c-f) Positive samples (Baijiu with detectable contaminants). The blue line represents Baijiu + Ag cluster@rGO, and the pink line represents Baijiu + BPA(10^{-8} M) + Ag cluster@rGO.

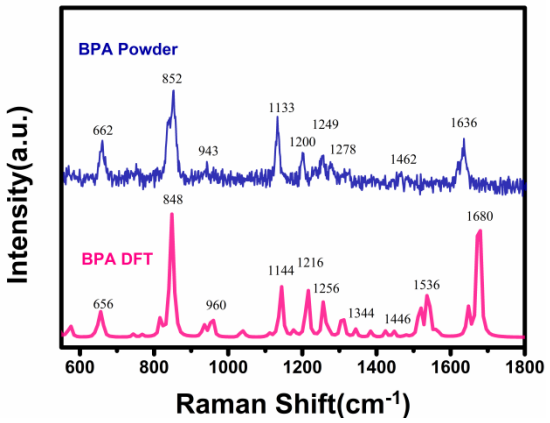

Figure S13. The SERS spectra of BPA Power (blue line) and the theoretical Raman spectrum of BPA (pink line).

Section S9.

There are some differences in the measured Raman characteristic peaks from various samples (**Figure 7d**), owing to the different adsorption modes between the BPA and SERS substrate in various samples. To prove that the measured peaks are actually from the same BPA, ten random BPA standard samples were selected and detected via our designed Ag cluster@rGO substrate.

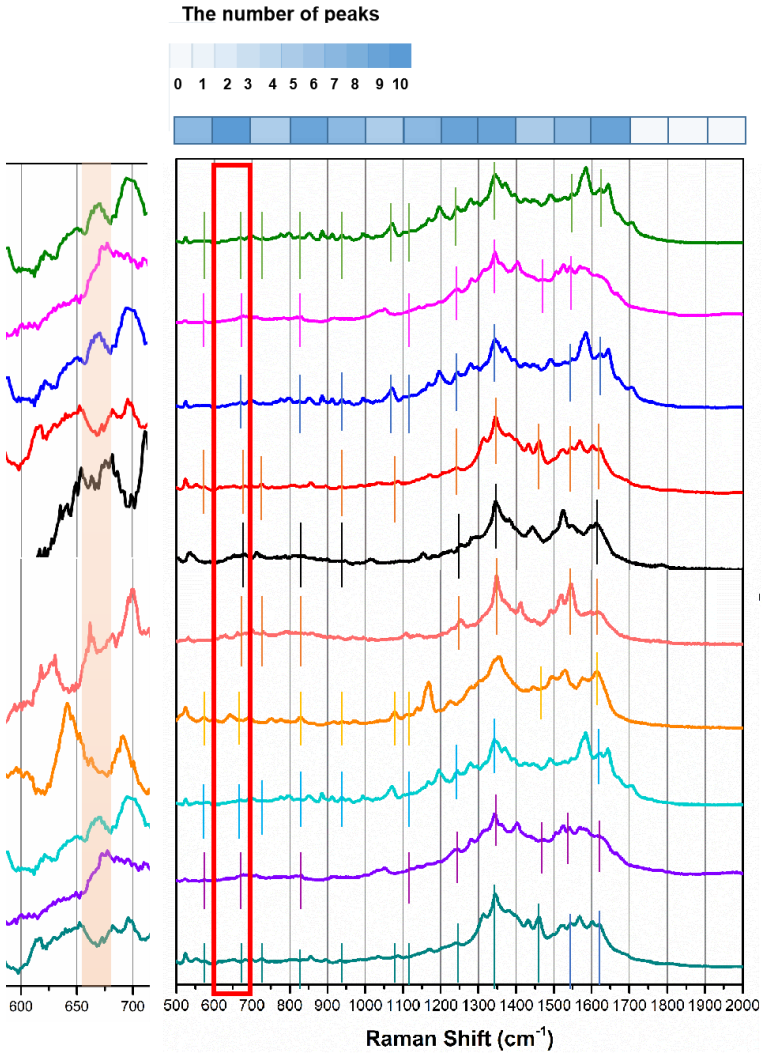

Figure S14. SERS spectra of ten random BPA standard samples. (The left image represents the enlargement of 600-700 cm^{-1}, the blue gradient color blocks respectively represent the number of peaks of 10 samples in a specific area in the interval.)

The obtained SERS spectra have been further analyzed via dividing the range between 500-200 cm^{-1} into 15 smaller domains. During each same domain, the characteristic peaks were marked via vertical lines in different colors. For instance,

during the enlargement range between 600-700 cm^{-1} illustrated in the left of **Figure S14**, it can be found that the width of each characteristic peak is about 20-30 cm^{-1} but same, thus the characteristic peaks during such domain are within the range of 655-685 cm^{-1}. The blue gradient color blocks respectively represent the number of peaks of 10 samples in a specific area in the interval. Therefore, when the characteristic peak appears in this range, we can label it as the characteristic peak of BPA, and the same way for other intervals.

Section S10. HPLC-MS/MS detection of BPA in Baijiu.

1. Apparatus

Shimadzu LCMS-8050 equipped with an electrospray ionisation source (ESI).

2. Chromatographic conditions

Separation was performed at 40 ℃ on a reverse-phase column (Shimadzu Shim-pack Scepter C18 (100 × 2.0 mm. i.d, 1.9μm particle size).The mobile phase was prepared by mixing 0.05 % ammonia solution (A) and methanol (B). The binary gradient program employed was the following: isocratic conditions for the first 1.5 min: 90% A and 10%B ; (2) linear gradientfrom 1.5 to 2 min with the final conditions being 60%A and 40%B and then isocratic conditions from 2 to 4 min; (3) linear gradient from 4 to 8 min with the final conditions being 40 % A and 60%; (4) linear gradient from 8 to 15 min with the final conditions being 5%A and 95% and then isocratic conditions from 15 to 17 min; (5) linear gradient from 17 to 17.1 min with the final conditions being 90%A and 10% and then isocratic conditions from 17.1 to20 min; Injection volume: 10 μL (Co-injection with water).

3. Mass spectrometry

Mass spectrometric detection was performed with Shimadzu LCMS-8050 equipped with an electrospray ionisation interface (ESI). Analytes were detected by multiple reaction monitoring mode (MRM) using electrospray ionisation (negative polarity). The MS source parameters were the following: Heat block temperature: 300 ℃, Drying gas (N2):10 L/min, Heating gas (N2):10 L/min.

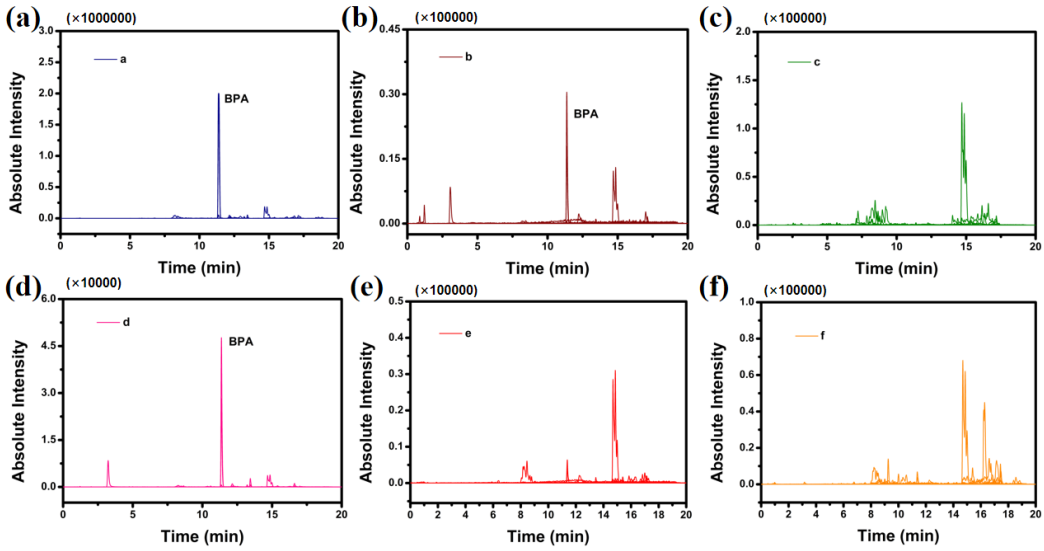

Figure S15. HPLC-MS/MS detection of six types of Baijiu. (a) Positive sample a (The content of BPA is about 30 μg/L). (b) Positive sample b (The content of BPA is about 4 μg/L). (c) Negative samples c (Not detected BPA or less than 1 μg/L). (d) Positive sample d (The content of BPA is about 2.5 μg/L). (e-f) Negative samples (Not detected BPA or less than 1 μg/L).

The detection limit of BPA by HPLC-MS/MS is 10^{-8}M, and our Ag cluster@rGO substrate detection limit of BPA is 10^{-10}M. Baijiu sample c was not detected in the HPLC-MS/MS. However, the detection of low concentration of BPA Baijiu sample c was achieved by the Ag cluster@rGO substrate, which is sufficient to prove the ultra-sensitive property of our SERS substrate.

Section S11. SERS detection of BPA Powder.

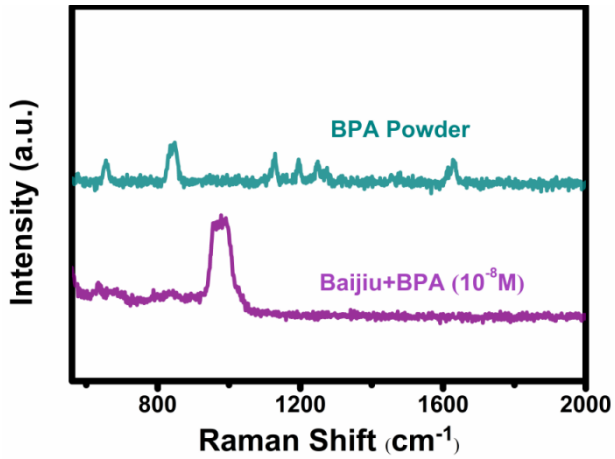

Figure S16. SERS spectrum of BPA Powder and Baijiu+BPA (10^{-8}M).